Experimental Quantum Simulation of Entanglement in Many-Body Systems

Jingfu Zhang,[1] Tzu-Chieh Wei,[1,3] and Raymond Laflamme[1,2]

[1]*Institute for Quantum Computing and Department of Physics, University of Waterloo, Waterloo, Ontario, Canada N2L 3G1*
[2]*Perimeter Institute for Theoretical Physics, Waterloo, Ontario, N2J 2W9, Canada*
[3]*Department of Physics and Astronomy, University of British Columbia, Vancouver, British Columbia V6T 1Z1, Canada*

(Received 2 April 2011; revised manuscript received 8 May 2011; published 30 June 2011)

We employ a nuclear magnetic resonance (NMR) quantum information processor to simulate the ground state of an *XXZ* spin chain and measure its NMR analog of entanglement, or pseudoentanglement. The observed pseudoentanglement for a small-size system already displays a singularity, a signature which is qualitatively similar to that in the thermodynamical limit across quantum phase transitions, including an infinite-order critical point. The experimental results illustrate a successful approach to investigate quantum correlations in many-body systems using quantum simulators.

DOI: 10.1103/PhysRevLett.107.010501 PACS numbers: 03.67.Ac, 03.67.Lx, 75.10.Pq

Entanglement, delineated as a nonlocal correlation, is one "spooky" characteristic trait of quantum mechanics [1]. The famous dispute between Bohr and Einstein on the fundamental question of quantum mechanics, the Schrödinger cat paradox, and the transitions from quantum to classical worlds essentially involve entanglement. The recent development of quantum information has rekindled interest in entanglement, more as a possible resource for information processing [2]. Various methods have been proposed to characterize entanglement qualitatively and quantitatively [3]. One immediate application of entanglement is the investigation of quantum phase transitions (QPTs) [4–6] in many-body systems, which occur at zero temperature ($T = 0$ K), where the transitions are driven by quantum fluctuations and the ground-state wave function is expected to develop a drastic change. The entanglement properties extend and complement the traditional statistical-physical methods for QPTs, such as correlation functions and low-lying excitation spectra. However, how to describe and measure entanglement in many-body systems is still a challenging task in both theoretical and experimental aspects [7,8]. Most schemes for directly measuring entanglement focus on the entanglement between two qubits [9,10]. Although the degree of entanglement for a medium-size or lager system can in principle be probed [8,11], it has not been experimentally measured directly.

In contrast to classical approaches, quantum simulators [12] provide a promising approach for investigating many-body systems and enable one to efficiently simulate other quantum systems by actively controlling and manipulating a certain quantum system, and to test, probe, and unveil new physical phenomena. One interesting aspect is to simulate the ground states of many-body systems, where usually rich phases can exist, such as ferromagnetism, superfluidity, and quantum Hall effect, just to name a few. In this Letter we experimentally simulate the ground state of an *XXZ* spin chain [13] in a liquid-state nuclear magnetic resonance (NMR) quantum information processor [14] and directly measure a global multipartite entanglement—the geometric entanglement (GE) [15,16] in a version of NMR analog, or pseudoentanglement. Exploiting the probed behavior of GE, we identify two QPTs, which in the thermodynamic limit correspond to the first and ∞ orders, respectively. In the ∞-order QPT, also known as Kosterlitz-Thouless (KT) transition [17,18], the ground-state energy is *not* singular. Consequently, the detection of the critical point in the KT transition may pose a challenge for correlation-based approaches [5,19], which rely on the singularity of ground-state energy. Surprisingly, the GE turns out to be nonanalytical but of different types of singularity at the first- and ∞-order transitions [20]. Remarkably, the qualitative features of ground-state entanglement in the thermodynamic limit displayed near both transitions persist even for a small-size system, on which our experiment is performed.

The GE of a pure many-spin quantum state $|\Phi\rangle$ is captured by the maximal overlap [15,16] $\Lambda_{\max} \equiv \max_{\Psi}|\langle\Psi|\Phi\rangle|$, and is defined as $E_{\log_2} = -\log_2\Lambda^2_{\max}$, where $|\Psi\rangle \equiv \bigotimes_{i=1}^{N}|\psi^{(i)}\rangle$ denotes all product (i.e., unentangled) states of the N-spin system. From the point of view of local measurements, the GE is essentially (modulo a logarithmic function) the maximal probability that can be achieved by a local projective measurement on every site, and the closest product state signifies the optimal measurement setting. The GE has been employed to study QPTs [16,21], local state discrimination [22], and entanglement as computational resources [23].

The *XXZ* spin chain is described by the Hamiltonian

$$H_{XXZ} = \sum_{i=1}^{N}(X_iX_{i+1} + Y_iY_{i+1} + \gamma Z_iZ_{i+1}), \qquad (1)$$

where X_i, Y_i, Z_i denote the Pauli matrices with i indicating the spin location, and γ is the control parameter for QPTs. We use the periodic boundary condition with $N + 1 \equiv 1$. The *XXZ* chain can be exactly solved by the so-called

Bethe ansatz and exhibits rich phase diagrams in the ground state [13]. In the thermodynamic limit, for $\gamma < -1$, the system has the ground state with the ferromagnetic (FM) Ising phase. At $\gamma = -1$ a first-order QPT occurs. For $-1 < \gamma \leq 1$, the system is in a gapless phase or XY-like phase. At $\gamma = 1$ there is an ∞ order or a KT transition [17], where the ground-state energy, however, is analytic across the transition, and so is any correlation function. For $\gamma > 1$, the system is in the Néel-like antiferromagnetic (AFM) phase. The ground state is asymptotically doubly degenerate. However, the excitations above the ground space have a gap. For $\gamma \gg 1$, the ground state takes a Néel or Ising AFM state, i.e., $|\ldots 10101010\ldots\rangle$, where $|0\rangle \equiv |\uparrow\rangle$ and $|1\rangle \equiv |\downarrow\rangle$.

In the XXZ chain (1), the GE displays a jump across $\gamma = -1$ but a cusp (i.e., the derivative is discontinuous) across $\gamma = 1$ [20]. Both features are present for small-size systems, as well as in the thermodynamic limit. For $\gamma < -1$ the GE is essentially zero. Regardless of the system size (as long as it is even), for $-1 < \gamma \leq 1$, the closest product state is found to be $|+-+-\ldots\rangle$, whereas for $\gamma \geq 1$, the closest product state is found to be $|0101\ldots\rangle$, where $|\pm\rangle \equiv (|0\rangle \pm |1\rangle)/\sqrt{2}$ [24]. Right at the KT point $\gamma = 1$, because of rotational symmetry, the closest product states are $|\phi\phi^{\perp}\phi\phi^{\perp}\ldots\rangle$, where $|\phi\rangle$ and $|\phi^{\perp}\rangle$ are any arbitrary orthonormal qubit states. The singular behavior of ground-state GE can be used to probe the KT transition, and there is no need to know the low-lying spectrum.

In implementation we use a 4-spin chain. The entanglement features pertinent to the QPTs in the thermodynamic limit will survive. The ground-state energy and wave function of the 4-spin chain are represented as (see supplemental material [25])

$$E_g = \begin{cases} 4\gamma & (\gamma < -1), \\ -2\gamma - 2\sqrt{\gamma^2 + 8} & (\gamma > -1), \end{cases} \tag{2}$$

$$|g\rangle = \begin{cases} |1111\rangle & (\gamma < -1), \\ |\phi_1\rangle \cos\alpha + |\phi_2\rangle \sin\alpha & (\gamma > -1), \end{cases} \tag{3}$$

where $\alpha \in (-\pi/2, 0)$ is given via $\tan(2\alpha) = -2\sqrt{2}/\gamma$, and $|\phi_1\rangle \equiv (|0101\rangle + |1010\rangle)/\sqrt{2}$, $|\phi_2\rangle \equiv (|1100\rangle + |0011\rangle + |1001\rangle + |0110\rangle)/2$. Figure 1(a) shows E_g as a function of γ. One should note that E_g is continuous at $\gamma = -1$ while the ground state $|g\rangle$ is discontinuous.

In order to obtain the ground-state GE, one needs to search for the closest product state $|\Psi^*\rangle$ [20]. In fact, we can choose the product states

$$|\Psi^*(\gamma)\rangle = \begin{cases} |\Psi_1\rangle \equiv |1111\rangle & (\gamma < -1) \\ |\Psi_2\rangle \equiv |+-+-\rangle & (-1 < \gamma < 1) \\ |\Psi_3\rangle \equiv |0101\rangle & (\gamma > 1) \end{cases} \tag{4}$$

to obtain the corresponding entanglement in the respective range of γ. To anticipate the experimental procedure, we shall measure the ground-state overlap listed as

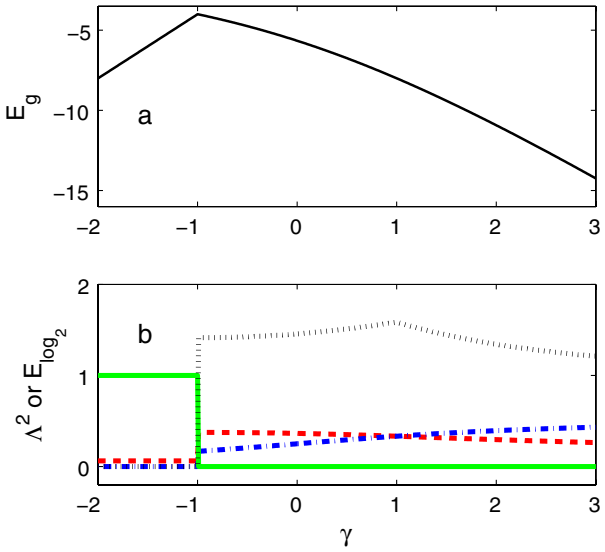

FIG. 1 (color online). Theoretical results in the 4-spin XXZ chain. (a) Energy level of the ground state. (b) The overlap square $\Lambda_i^2(\gamma)$ and entanglement $E_{\log_2}(\gamma)$. The solid, dashed, and dash-dotted curves show $\Lambda_i^2(\gamma)$ for $|\Psi_1\rangle = |1111\rangle$, $|\Psi_2\rangle = |+-+-\rangle$, and $|\Psi_3\rangle = |0101\rangle$, respectively. $E_{\log_2}(\gamma)$ is shown as the dotted curve. The jump at $\gamma = -1$ and the cusp at $\gamma = 1$ in $E_{\log_2}(\gamma)$ indicate the transition points for the QPTs, with the first and ∞ orders, respectively.

$$\Lambda_1(\gamma) = \langle\Psi_1|g\rangle = \begin{cases} 1 & (\gamma < -1) \\ 0 & (\gamma > -1) \end{cases} \tag{5}$$

$$\Lambda_2(\gamma) = \langle\Psi_2|g\rangle = \begin{cases} \frac{1}{4} & (\gamma < -1) \\ \frac{\sqrt{2}}{4}\cos\alpha - \frac{1}{2}\sin\alpha & (\gamma > -1) \end{cases} \tag{6}$$

$$\Lambda_3(\gamma) = \langle\Psi_3|g\rangle = \begin{cases} 0 & (\gamma < -1) \\ \frac{1}{\sqrt{2}}\cos\alpha & (\gamma > -1). \end{cases} \tag{7}$$

From Eqs. (6) and (7), one finds that $\Lambda_2(\gamma)$ and $\Lambda_3(\gamma)$ cross at $\gamma = 1$. Figure 1(b) shows the theoretical prediction for $\Lambda_i^2(\gamma)$ $(i = 1, 2, 3)$ and the entanglement $E_{\log_2}$. The jump in the entanglement at $\gamma = -1$ and the cusp at $\gamma = 1$ signify the two QPT points.

In experiment, we choose the four carbons in crotonic acid [26] dissolved in d6 acetone as the four qubits. We generate the ground states using quantum networks and implement the quantum gates by GRAPE pulses [27]. Various ground states can be created by varying the single spin rotations that can be easily implemented (see supplemental material [25]). In principle, one can employ an iterative method to experimentally measure the GE of the ground state (see supplemental material [25]). To demonstrate the proof-of-principle simulation of quantum entanglement, instead, we first measure the overlap of the ground state with several product states (4), which contain the closest product states. From the measurement with the already known closest product states, we can obtain the

ground-state GE. Next, to show that the obtained results are the optimum, we vary the product states to test the optimality.

The experimentally measured $\Lambda_i^2(\gamma)$ for various γ are shown in Fig. 2(a). The measured $\Lambda_i^2(\gamma)$ for $\gamma < -1$ are 0.92, 0.048, and 0.019, indicated as the dotted, dashed, and dash-dotted lines. The corresponding theoretical values are 1, 1/16, and 0, respectively. In the region $\gamma > -1$, $\Lambda_1^2(\gamma)$ can be fitted as $\Lambda_1^2(\gamma) = 0.014$, shown as the dotted line, corresponding to 0 in theory.

We perform polynomial fits to the measured $\Lambda_2^2(\gamma)$ and $\Lambda_3^2(\gamma)$, and obtain the two solid curves that cross at the point $\gamma = 0.92$, which is very close to the theoretically predicted transition point at $\gamma = 1$. The discrepancy between experiment and theory mainly comes from the different experimental errors in measuring $\Lambda_2^2(\gamma)$ and $\Lambda_3^2(\gamma)$.

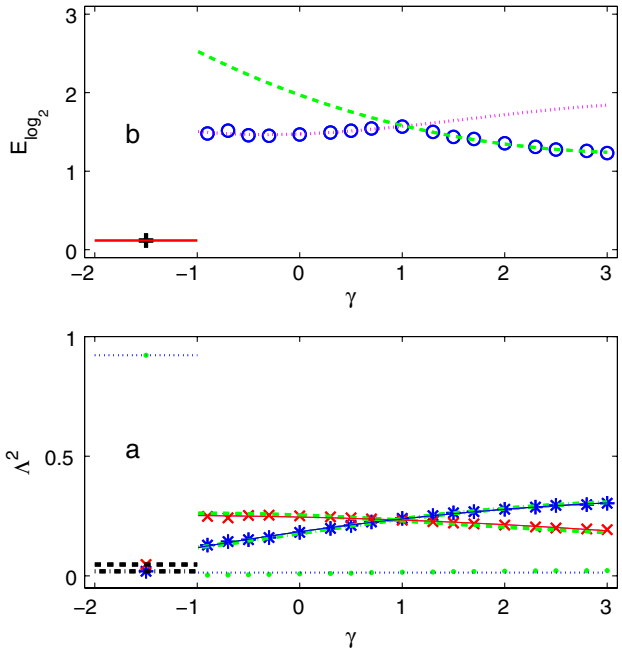

FIG. 2 (color online). Experimentally measured $\Lambda_i^2(\gamma)$ (a) and $E_{\log_2}$ (b) for various γ. In figure (a), the experimental data are shown as ●, × and * for $\Lambda_i^2 = |\langle\Psi_i|g\rangle|^2$, corresponding to $|\Psi_1\rangle$, $|\Psi_2\rangle$, and $|\Psi_3\rangle$. The measured $\Lambda_i^2(\gamma)$ for $\gamma < -1$ are indicated as the dotted, dashed, and dash-dotted lines. In the region $\gamma > -1$, $\Lambda_1^2(\gamma)$ can be fitted as the dotted line. Through fitting the points for $\Lambda_2^2(\gamma)$ and $\Lambda_3^2(\gamma)$ using polynomial functions, we obtain the two solid curves that cross at point $\gamma = 0.92$, close to the theoretical point at $\gamma = 1$. The thick dashed and dash-dotted curves show the fitting results using the theoretical $\Lambda_2^2(\gamma)$ and $\Lambda_3^2(\gamma)$ by introducing decay factors 0.69 and 0.71, respectively. In (b), in the region $\gamma < -1$, $E_{\log_2}$ is shown as +. For $\gamma > -1$, we rescale the measured $\Lambda_2^2(\gamma)$ and $\Lambda_3^2(\gamma)$ as $\Lambda_2^2(\gamma)/0.69$ and $\Lambda_3^2(\gamma)/0.71$, respectively. The dotted and dashed curves that cross at $\gamma = 1.02$ show the fitting results of the rescaled data using polynomial functions. The expected $E_{\log_2}$ after rescaling is indicated by ○.

The jump at $\gamma = -1$ and the cusp at $\gamma = 0.92$ reflect the different types of QPT points.

In order to faithfully estimate the performance of the experiment in measuring $\Lambda_2^2(\gamma)$ and $\Lambda_3^2(\gamma)$ in the region $\gamma > -1$, we introduce two decay factors α_2 and α_3 to fit the experimental data as $[\Lambda_{2,3}^2(\gamma)]_{\text{exp}} = \alpha_{2,3}[\Lambda_{2,3}^2(\gamma)]_{\text{theory}}$, shown as the thick dashed and dash-dotted curves in Fig. 2(a) with the best scale factors as $\alpha_2 = 0.69$ and $\alpha_3 = 0.71$, respectively. The difference between the decay factors comes from the different operations in measuring $\Lambda_2^2(\gamma)$ and $\Lambda_3^2(\gamma)$. In Fig. 2(b), we exploit the decay factors to rescale experimental values of $[\Lambda_{2,3}^2]_{\text{exp}}/\alpha_{2,3}$, from which we obtain the expected values of pseudoentanglement shown as ○. The rescaled $-\log_2([\Lambda_{2,3}^2]_{\text{exp}}/\alpha_{2,3})$ can be fitted as the dotted and dashed curves that cross at $\gamma = 1.02$.

In principle, we do not need to know the closest product states in order to measure the entanglement. In the supplemental material [25], we describe an iterative procedure to search for them and this procedure can be implemented in experiment. For proof-of-principle demonstration of the optimality experimentally, we simplify the procedure and vary the product states $|\Psi(\beta)\rangle$ by

$$|\Psi(\beta)\rangle = U_p(\beta)|0101\rangle, \tag{8}$$

where $U_p(\beta) = \bigotimes_{j=1}^4 e^{-i\beta Y_j/2}$, and experimentally measure $\Lambda^2 = |\langle\Psi(\beta)|g\rangle|^2$ for various β at three different locations of the phase diagram, corresponding to $\gamma = -0.9$, 1, and 3, respectively. The theoretical and experimental results are shown in Figs. 3(a) and 3(b), respectively. The experimental data are compared to the theoretical values of $0.66\Lambda^2$, $0.68\Lambda^2$, and $0.71\Lambda^2$, shown in Fig. 3(b). One finds that the maximum of Λ^2 occurs at $\beta = \pi/2$ and 0 for $\gamma = -0.9$ and 3, respectively. These correspond to the respective closest product states, $|\Psi_2\rangle = |+-+-\rangle$ and $|\Psi_3\rangle = |0101\rangle$, predicted theoretically. Remarkably, for $\gamma = 1$, where the ∞-order QPT occurs, Λ^2 is a constant independent of β, as we have expected and noted earlier. This also means that arbitrary states prepared by Eq. (8) can be chosen to measure the entanglement at $\gamma = 1$, and this gives additional confirmation that the created state at the KT point is rotationally invariant.

The experiment duration of the preparation of the ground states for $\gamma > -1$ is about 160 ms, which is non-negligible (about 17%) compared to the coherence time T_2. Consequently, the decay of the signals due to the limitation of coherence time is one of the main sources of errors. Additionally, the imperfection of pulses and inhomogeneities of magnetic fields also contributes to errors. The deviations of the experimental data from the theoretical fitting in Fig. 3(b) represent the effects of the errors that depend on the rotation angles, or the product states. In particular the fluctuation of the data for $\gamma = 1$ in Fig. 3(b) confirms the explanation for the shift of the measured cusp in Fig. 2(a).

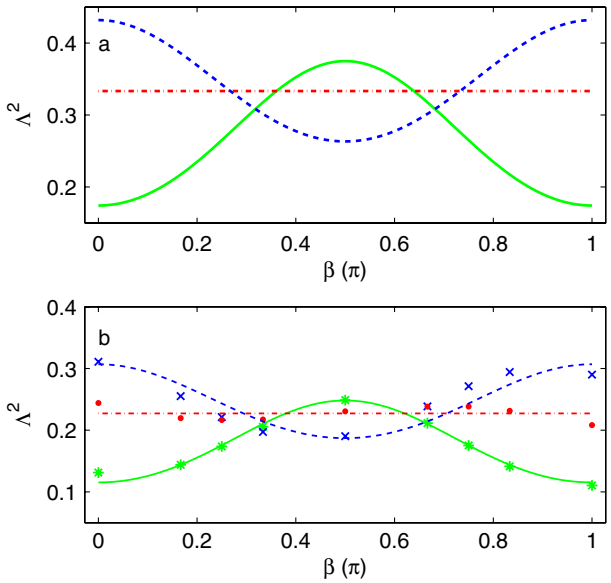

FIG. 3 (color online). Theoretical (a) and experimentally measured (b) Λ^2 for various product states created as $U_p(\beta)|0101\rangle$ [see Eq. (8)]. Three ground states for $\gamma = -0.9$, 1, and 3 are chosen and the corresponding Λ^2 are shown as the solid, dash-dotted, and dashed curves in (a), respectively. The experimental data are shown as *, ●, and × for $\gamma = -0.9$, 1, and 3 in (b), respectively. In comparison with the theoretical values, they can be fitted as $0.66\Lambda^2$, $0.68\Lambda^2$, and $0.71\Lambda^2$, shown as the solid, dash-dotted, and dashed curves.

In conclusion, we demonstrate the nonanalytic properties of many-body systems in a quantum simulator using NMR. The QPTs with first and ∞ orders in the XXZ spin chain are detected by directly measuring the pseudoentanglement of the ground states created by quantum gates. An alternative approach for creating ground states would be via adiabatic evolution [28]. Our preliminary numerical analysis indicates that ground states for $\gamma > -1$ can be approximately generated with high fidelity (e.g., >0.998) by the adiabatic evolution from the ground state at a large γ. The experimental implementation is a possible future direction.

We thank O. Moussa and R. Orús for helpful discussions. This work was supported by CIFAR (R. L.), NSERC (J.-F. Z., R. L., and T.-C. W.), MITACS (T.-C. W.), SHARCNET (R. L.), and QuantumWorks (R. L.).

[1] A. Einstein, B. Podolsky, and N. Rosen, Phys. Rev. **47**, 777 (1935).
[2] M. Nielsen and I. Chuang, *Quantum Computation and Quantum Information* (Cambridge University Press, Cambridge, U.K., 2000).
[3] R. Horodecki *et al.*, Rev. Mod. Phys. **81**, 865 (2009).
[4] S. Sachdev, *Quantum Phase Transitions* (Cambridge University Press, Cambridge, U.K., 2000).
[5] A. Osterloh *et al.*, Nature (London) **416**, 608 (2002).
[6] S. Sachdev, Nature Phys. **4**, 173 (2008).
[7] L. Amico *et al.*, Rev. Mod. Phys. **80**, 517 (2008).
[8] O. Gühne and G. Tóth, Phys. Rep. **474**, 1 (2009).
[9] P. Horodecki, Phys. Rev. Lett. **90**, 167901 (2003); H. A. Carteret, *ibid.* **94**, 040502 (2005).
[10] S. P. Walborn *et al.*, Nature (London) **440**, 1022 (2006); C. Schmid *et al.*, Phys. Rev. Lett. **101**, 260505 (2008).
[11] O. Gühne, M. Reimpell, and R. F. Werner, Phys. Rev. Lett. **98**, 110502 (2007).
[12] R. P. Feynman, Int. J. Theor. Phys. **21**, 467 (1982); S. Lloyd, Science **273**, 1073 (1996); I. Buluta and F. Nori, *ibid.* **326**, 108 (2009).
[13] V. E. Korepin *et al.*, *Quantum Inverse Scattering Method and Correlation Functions* (Cambridge University Press, Cambridge, 1997).
[14] L. M. K. Vandersypen and I. L. Chuang, Rev. Mod. Phys. **76**, 1037 (2005); J. A. Jones, Prog. Nucl. Magn. Reson. Spectrosc. **38**, 325 (2001).
[15] T.-C. Wei and P. M. Goldbart, Phys. Rev. A **68**, 042307 (2003).
[16] T.-C. Wei *et al.*, Phys. Rev. A **71**, 060305(R) (2005).
[17] J. M. Kosterlitz and D. J. Thouless, J. Phys. C **6**, 1181 (1973).
[18] C. C. Rulli and M. S. Sarandy, Phys. Rev. A **81**, 032334 (2010).
[19] L.-A. Wu, M. S. Sarandy, and D. A. Lidar, Phys. Rev. Lett. **93**, 250404 (2004); S.-J. Gu, Int. J. Mod. Phys. B **24**, 4371 (2010).
[20] R. Orús and T.-C. Wei, Phys. Rev. B **82**, 155120 (2010).
[21] R. Orús, Phys. Rev. Lett. **100**, 130502 (2008); R. Orús, S. Dusuel, and J. Vidal, *ibid.* **101**, 025701 (2008).
[22] M. Hayashi *et al.*, Phys. Rev. Lett. **96**, 040501 (2006).
[23] D. Gross, S. T. Flammia, and J. Eisert, Phys. Rev. Lett. **102**, 190501 (2009).
[24] Here $|+-+-\ldots\rangle$ is equivalent to $|-+-+\ldots\rangle$ or more generally $|\theta_+\theta_-\theta_+\theta_-\ldots\rangle$ with $\theta_\pm \equiv (|0\rangle \pm e^{i\theta}|1\rangle)/\sqrt{2}$ due to the symmetry in the ground states. Similarly, $|1010\ldots\rangle$ is equivalent to $|0101\ldots\rangle$.
[25] See supplemental material at http://link.aps.org/supplemental/10.1103/PhysRevLett.107.010501 for details regarding (1) solving the 4-spin XXZ chain, (2) an iterative method for computing the GE and experimentally measuring it without prior knowledge of closest product states, and (3) further discussions on experimental implementation.
[26] E. Knill *et al.*, Nature (London) **404**, 368 (2000).
[27] N. Khaneja *et al.*, J. Magn. Reson. **172**, 296 (2005); C. A. Ryan *et al.*, Phys. Rev. A **78**, 012328 (2008).
[28] P. Král, I. Thanopulos, and M. Shapiro, Rev. Mod. Phys. **79**, 53 (2007); X. Peng *et al.*, Phys. Rev. Lett. **103**, 140501 (2009).